Journal of Alloys and Compounds 509 (2011) 5285–5289

Contents lists available at ScienceDirect

Journal of Alloys and Compounds

journal homepage: www.elsevier.com/locate/jallcom

An optimized multilayer structure of CdS layer for CdTe solar cells application

Junfeng Han[a,b], Cheng Liao[a,*], Tao Jiang[a], C. Spanheimer[b], G. Haindl[b], Ganhua Fu[b], V. Krishnakumar[b], Kui Zhao[a], A. Klein[b], W. Jaegermann[b]

[a] State Key Laboratory of Nuclear Physics and Technology, School of Physics, Peking University, Road Yiheyuan 5, Beijing 100871, China
[b] Institute of Materials Science, Darmstadt University of Technology, Petersenstr. 23, 64287 Darmstadt, Germany

ARTICLE INFO

Article history:
Received 16 July 2010
Received in revised form
11 November 2010
Accepted 14 December 2010
Available online 22 December 2010

Keywords:
CdTe solar cells
CBD
CSS
Multilayer CdS

ABSTRACT

CdS layers grown by 'dry' (close space sublimation) and 'wet' (chemical bath deposition) methods are deposited and analyzed. CdS prepared with close space sublimation (CSS) has better crystal quality, electrical and optical properties than that prepared with chemical bath deposition (CBD). The performance of CdTe solar cell based on the CSS CdS layer has higher efficiency than that based on CBD CdS layer. However, the CSS CdS suffers from the pinholes. And consequently it is necessary to prepare a 150 nm thin film for CdTe/CdS solar cell. To improve the performance of CdS/CdTe solar cells, a thin multilayer structure of CdS layer (~80 nm) is applied, which is composed of a bottom layer (CSS CdS) and a top layer (CBD CdS). That bi-layer film can allow more photons to pass through it and significantly improve the short circuit current of the CdS/CdTe solar cells.

Crown Copyright © 2010 Published by Elsevier B.V. All rights reserved.

1. Introduction

CdS is one of the group II–VI compound semiconductors with a direct optical band gap of 2.42 eV, used as a suitable window layer for CdTe based photovoltaic devices [1]. The CdS/CdTe contact is the energy converting interface in the CdTe solar cell [2,3]. The electrical and the structural properties of the CdS layers can influence the characteristics of CdS/CdTe heterojunction interface and consequently the performance of the whole cells [4]. The study of CdS/CdTe interface is necessary and important [5,6].

Chemical bath plating is in most widespread use. It is a wet chemical method based on the slow, controlled decomposition of thiourea in alkaline solution and the presence of Cd^{2+} ions [7–9]. 16.5% efficiency of CdS/CdTe solar cell was achieved by NREL with CBD CdS [10]. Although CBD CdS films have high photoconductivity and morphological properties, they tend to form the cubic phase and thus poor crystalline quality [11,12]. Close space sublimation (CSS) is another popular way to deposit CdS films, which is easy to get higher quality crystal with higher substrate temperature and less impurity in the films [13,14]. Also CSS is a relatively inexpensive technique for deposition of polycrystalline thin film due to simple configuration [15].

The performance of CdTe solar cells is strongly limited by the thickness of CdS [16,17]. Though higher short circuit current can be achieved by reducing the CdS thickness directly, it usually severely reduces device open circuit voltage and fill factor because single thin CSS CdS films suffer from pinholes and shorts among grain boundaries. Ideally, the CdS films should be thin enough to allow high transmission and uniform to avoid short circuit effects [9]. This requirement can be obtained with multilayer CdS [18]. The second layer (CBD CdS) is composed of small grains and is expected to fill the pinholes. The multilayer CdS film is more compact and uniform than a single CSS CdS layer.

In this work, multilayer CdS films were prepared as an improvement of the window layer. The total thickness of multilayer CdS is about 80 nm, which can allow more photons to pass through it and contribute to the photocurrent. CdS films were deposited by the CBD and CSS methods. Chemical, electronic, morphological and optical properties were investigated using X-ray photoelectron spectroscopy (XPS), X-ray diffraction (XRD), atomic force microscopy (AFM) and UV–vis spectroscopy.

2. Experimental

The substrates were $2 \times 2\ cm^2$ soda lime glasses coated with ITO. The substrates were cleaned in the isopropanol and DI-water respectively for 20 min with ultrasonic. Then they were dried out by nitrogen. The CSS CdS film was prepared in vacuum chamber. The vacuum of the system for close space sublimate method was below 1×10^{-7} mbar. The source temperature was 680 °C and the substrate was kept at 520 °C. A standard CSS CdS film (sample A) was deposited for 2 min, which was 150 nm thick. A standard CBD CdS film (sample B) was prepared in liquid chemical solution, which contained 1.5×10^{-3} mol/L cadmium acetate and 5×10^{-2} mol/L thiourea. Ammonia was employed to adjust the solution pH to 11 at room temperature. The bath temperature was kept constant at 75 °C for a deposition time of 60 min. The thickness of the standard CBD CdS film was around 150 nm. Sample

* Corresponding author. Tel.: +86 10 62751889; fax: +86 10 62758849.
E-mail addresses: pkuhjf@gmail.com (J. Han), Cliao@pku.edu.cn (C. Liao).

0925-8388/$ – see front matter. Crown Copyright © 2010 Published by Elsevier B.V. All rights reserved.
doi:10.1016/j.jallcom.2010.12.085

Table 1
The RMS of different CdS films: sample A, standard CSS CdS; sample B, standard CBD CdS; sample C, thin CSS CdS (60 nm); sample D, multilayer CdS (80 nm).

	Sample name			
	Sample A	Sample B	Sample C	Sample D
RMS/nm	10.4	4.0	4.9	3.4

C was deposited for 50 s with standard CSS process and the thickness was around 60 nm. Sample D was prepared with first standard CSS CdS process but reduced deposition time (50 s) and an additional standard chemical bath CdS layer as sample B. The reaction of the second course was kept at 75 °C for 10 min. The total thickness of the multilayer CdS film (sample D) was around 80 nm.

With all CdS films complete CdTe/CdS solar cell devices were fabricated. A 5 μm CdTe layer was deposited by close space sublimation at source and substrate temperatures of 600 °C and 520 °C respectively. This was followed by an ex situ CdCl2 treatment, NP etching and gold back contact deposition. Finally the 2×2 cm^2 coated glass sheets were scribed with stainless steel needles into cells of 5×5 mm^2 dimension.

Morphological properties of the samples were obtained by atomic force microscope using an AC mode (Asylum research MFP-3D). Optical properties were analyzed by UV–vis–IR transmittance (Perkin-Elmer Lambda 900). The crystallographic structure of the film was studied by X-ray diffraction (Rigaku). X-ray photoelectron spectroscopy (XPS) studies have been performed using an Escalab 250 spectrometer with a monochromatized Al anode X-ray source ($h\nu$ = 1486.6 eV). Performances of CdTe/CdS solar cells were characterised by J–V curve. The cell efficiency was measured under AM1.5 (100 mW/cm^2) illumination using a solar simulator.

3. Results and discussion

3.1. Morphology and structure

Table 1 shows the roughness of sample A (standard CSS CdS), sample B (standard CBD CdS), sample C (thin CSS CdS) and sample D (multilayer CdS). From AFM images (shown in Fig. 1), the grain sizes of sample A are much larger than sample B. The crystal quality of CSS CdS is better than that of CBD CdS film. However, more cracks among grain boundaries are found in the 3D picture of sample A. These are evidently the reason that the 150 nm thickness is necessary for CSS CdS layer. The grain sizes of sample C are smaller than that of sample A due to the less thickness. With the second CBD CdS layer (sample D) on top, which has a small grain size, no pinholes and cracks among grain boundaries are observed in the multilayer CdS. The surface is smoother than that of a single CSS CdS layer. As a window layer, the multilayer CdS is free of holes with a uniform grain size distribution which has a positive effect on the performance of the final device.

Fig. 2 shows XRD patterns for deposited standard CSS and CBD films respectively. The identification and assignment of the observed diffraction patterns are made using the JPDS data. The reflexes (1 0 2) at 36.6° and (1 0 3) at 47.9° belong to the hexagonal phase of CdS and appear only in the diffractogram of sample A (CSS CdS). That indicates CSS CdS is composed of stable hexagonal structure. The reflexes (2 2 0) at 44.2° in the sample B indicate that the CBD CdS layer has a structure mixed with the hexagonal and cubic phases, which is metastable compared with CSS CdS films. A narrower main peak (0 0 2) width of sample A is associated with a larger grain size than sample B, which is also shown in AFM pictures (Fig. 1).

3.2. Optical property

The optical transmittance spectra of different CdS films are shown in Fig. 3. The absorption edge of sample A is in the range from 500 nm to 520 nm, which is sharper than that of sample B in the range from 480 nm to 550 nm. The sharper absorption edge indicates that the CSS CdS film has better crystallinity than that of CBD CdS. Also this analysis indicates fewer defects and impurity energy levels in the CSS CdS film. The band gap (E_g) values can be calcu-

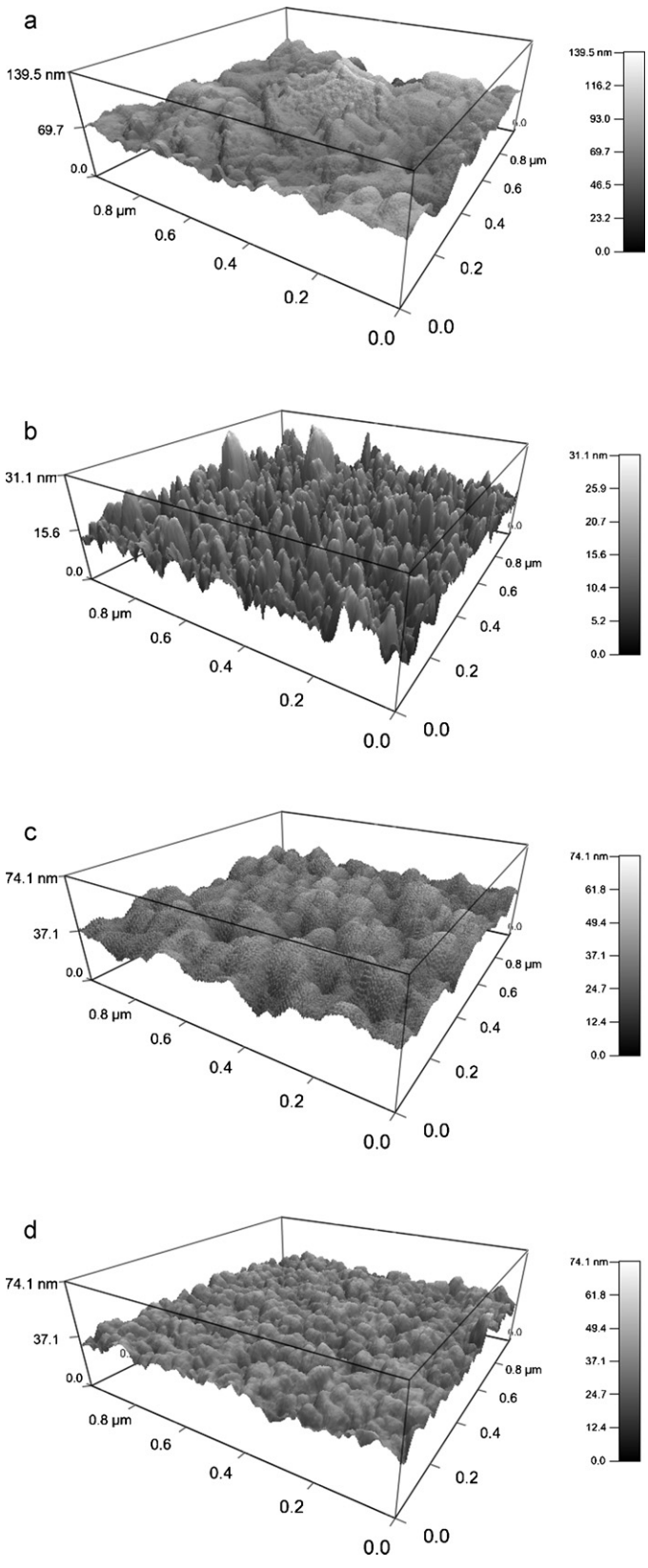

Fig. 1. AFM of different CdS films: sample A, standard CSS CdS; sample B, standard CBD CdS; sample C, thin CSS CdS (60 nm); sample D, multilayer CdS (80 nm).

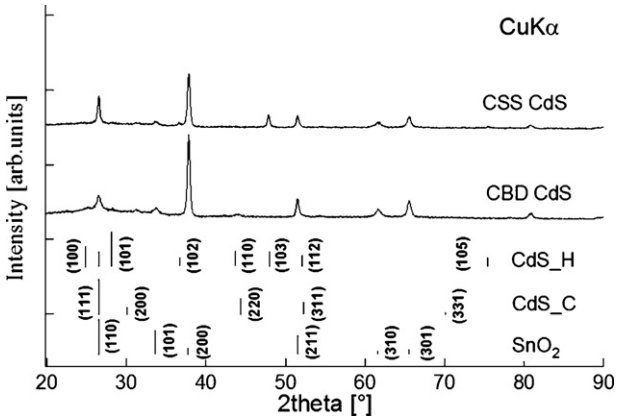

Fig. 2. XRD patterns for CSS and CBD CdS films: sample A, standard CSS CdS; sample B, standard CBD CdS.

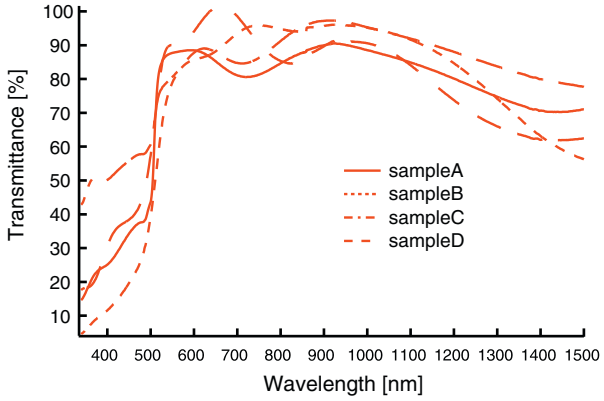

Fig. 3. Optical transmittance spectra for different CdS films: sample A, standard CSS CdS; sample B, standard CBD CdS; sample C, thin CSS CdS (60 nm); sample D, multilayer CdS (80 nm).

lated by plotting $(\alpha h\nu)^2$ against $h\nu$ of the graph at the beginning of band to band absorption and taking the intersection of the tangent to the $(\alpha h\nu)^2$ axis (shown in Fig. 4): E_g (sample A) = 2.42 eV, E_g (sample B) = 2.38 eV. Due to better crystal quality and larger grain sizes, the band gap of the CSS CdS film has almost the same value as bulk CdS, which can allow more photons in the short wavelength range pass through the layer. However, the thickness of sample A is not thin enough as a window layer of CdTe solar cell. From Fig. 3, thinner CdS layer, sample C (60 nm) and sample D (80 nm) has higher

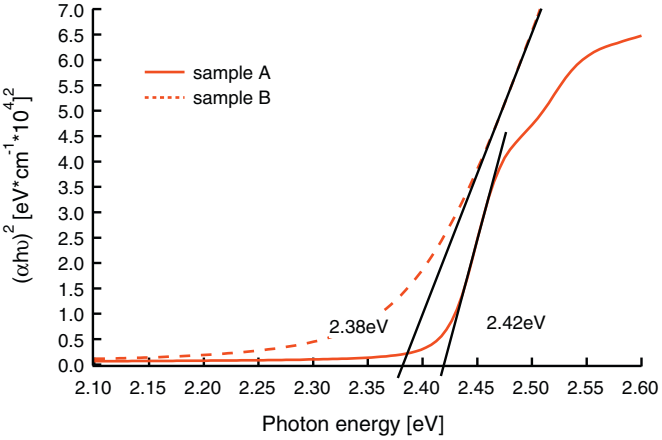

Fig. 4. Band gaps of different CdS films: sample A, standard CSS CdS; sample B, standard CBD CdS.

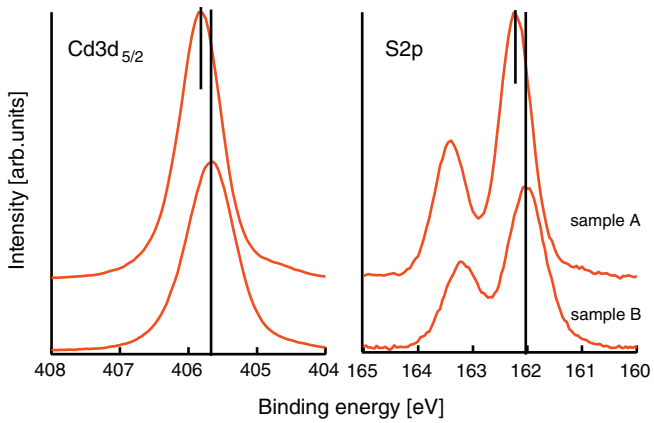

Fig. 5. X-ray photoelectron spectra of Cd3d5/2 and S2p core levels: sample A, standard CSS CdS; sample B, standard CBD CdS.

transmission at energies above E_g than sample A (150 nm) due to the less film thickness. Thereby more photons of the short wavelength range can pass through the window layer and contribute to the photocurrent.

3.3. XPS analysis

Surface electronic properties are analyzed by XPS. XP core level spectra of $Cd3d_{5/2}$ and S2p are shown in Fig. 5. Fermi level positions $(E_F - E_{VBM})$ of different CdS films can be calculated by subtracting the well known values for the difference of the substrate core levels with respect to the valence band maximum ($E_{Cd3d5/2} - E_{VBM}$ = 403.51 eV, $E_{S2p3/2} - E_{VBM}$ = 159.97 eV) from the measured core levels [19]. Table 2 gives binding energy values and Fermi level positions of sample A and sample B. The Fermi level of the CSS CdS film is closer to the conduction band than that of CBD CdS. Higher *n*-doping of the CdS layer leads to higher position of the Fermi level, which results in a higher band bending at the CdTe side. So the built in potential in the CdTe film is increased and consequently a higher open circuit voltage can be obtained. Also higher *n*-doping of the window layer can extend the depletion width in CdTe layer and increase the photoelectrons collection, which is benefit for the performance of solar cells.

In Fig. 6, the survey spectra of sample A and B indicate that the CBD CdS contains oxygen, which may be one reason of the low band gap of CBD CdS layer [20,21].

3.4. Performance of solar cells

Table 3 shows the performance of the solar cells. Sample D is the best solar cell of all samples. The short current density is 23.9 mA/cm^2, which is significantly higher than the other samples. The efficiency of sample D achieves 10.1%.

The performance of the solar cell based on the CSS CdS layer is better than that of CBD CdS layer. One reason of this improvement is attributed to the higher *n*-doping CdS layer and consequently higher built-in potential in the CdTe film. Also a higher *n*-type doping CdS can increase the depletion width in the CdTe, which can

Table 2
XP core levels and Fermi levels of different CdS films: sample A, standard CSS CdS; sample B, standard CBD CdS; sample C, thin CSS CdS (60 nm); sample D, multilayer CdS (80 nm).

Sample name	$Cd3d_{5/2}$ (eV)	$S2p_{3/2}$ (eV)	Fermi level (eV)
Sample A	405.85	162.25	2.34
Sample B	405.72	162.10	2.21

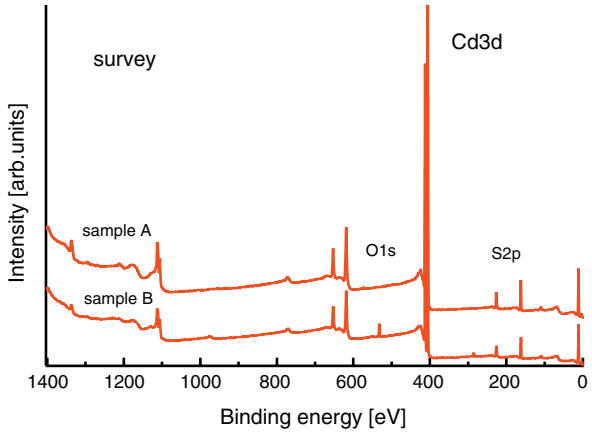

Fig. 6. X-ray photoelectron survey spectra of different CdS films. Sample A, standard CSS CdS; sample B, standard CBD CdS.

Table 3
Performances of CdS/CdTe solar cells with different CdS films: sample A, standard CSS CdS; sample B, standard CBD CdS; sample C, thin CSS CdS (60 nm); sample D, multilayer CdS (80 nm).

Sample name	V_{oc} (mV)	I_{sc} (mA/cm^2)	Fill factor (%)	Efficiency (%)
Sample A	723	21.1	63.0	9.63
Sample B	705	20.5	57.0	8.24
Sample C	465	15.0	37.6	2.62
Sample D	700	23.9	60.0	10.1

increase the collection of carriers and consequently higher photocurrent as indeed observed. Another reason is attributed to the better crystal quality and consequently higher optical transmittance and less recombination near the interface between CdTe and CdS.

Due to the lower CdS film thickness, sample C has higher optical transmittance at energies above E_g than the sample A. Thereby more photons of the short wavelength range can pass through the window layer and contribute to the photocurrent. However, in Fig. 7, the *J–V* curve of sample C shows poor performance. One possible reason may be more shunt paths and shorts due to the thinner window layer. Another reason is the inter-diffusion at the interface between CdTe and CdS. Nonuniform CdS consumption during the CdTe deposition and activation can result in lateral junction inhomogeneous, especially for cell structure with thinner CdS films. Sample D has less thickness than sample A, which can allow more photons pass through the window layer. With the second layer, it is more homogeneous and compact than single layer (sample C)

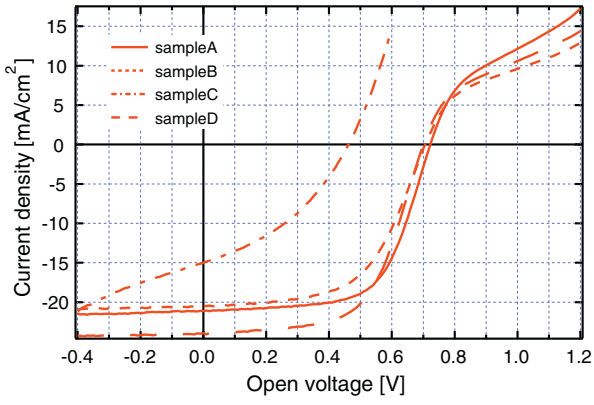

Fig. 7. *J–V* characteristics of CdS/CdTe solar cells with different CdS films. Sample A, standard CSS CdS; sample B, standard CBD CdS; sample C, thin CSS CdS (60 nm); sample D, multilayer CdS (80 nm).

as shown in Fig. 1. The solar cell based on sample D has not only almost the same open voltage and fill factor as sample A, but also higher short circuit current. It may be one way to obtain higher performance of the CdTe solar cell with multilayer CdS films.

4. Conclusion

The CdTe solar cells based on the standard CSS CdS and CBD CdS films achieves 9.63% and 8.24% efficiency respectively. The standard CBD CdS layer suffers from poor crystalline quality. The grain sizes of CBD CdS are smaller than that of CSS CdS film. Due to the large grain size, the surface roughness of CSS CdS layer is 10.4 nm, which is rougher than that of CBD CdS (4.0 nm). XRD patterns indicate that the CSS CdS layer is more like a hexagonal structure while the CBD CdS layer has a structure mixed with cubic and hexagonal phases. The main peak (0 0 2) of CSS CdS has decreased width due to larger grain sizes as shown in AFM picture. Optical transmittance spectrum shows steeper absorption edge, which indicates fewer defects in the film and better crystalline quality. Optical band gaps can be obtained from these transmittance spectrums. The band gap of CSS CdS film is 2.42 eV, the same as bulk CdS, while the band gap of CBD CdS film is only 2.38 eV. CSS CdS can allow more photons in the short wavelength range to pass through the window layer and contribute to the photocurrent. From the Cd and S XP core levels, the Fermi level in the CSS CdS layer shift towards the conduction band compared with that in the CBD CdS layer. It can be deduced that the shift causes a higher band bending in the CdTe and consequently increases the built-in potential, which is one reason for the higher performance of solar cell based on the CSS CdS layer.

It is difficult to achieve higher efficiency with the standard CSS CdS layer due to the thickness. A thin CdS layer can be obtained by reducing the deposition time. Higher transmission at energies above E_g is observed in the UV–vis transmittance spectra. However, the performance of solar cell based on such a thin CdS film is poor because more shunt paths and shorts in the thin CdS layer. Nonuniform CdS consumption during the inter-diffusion at the interface between CdTe and CdS can cause the junction inhomogeneous, especially for cell structure with thinner CdS films. In multilayer structure, the second layer can fill the grain boundaries and make the film more smooth, homogeneous and compact. This structure is very effective in the CdTe solar cells and a higher performance is obtained by this way.

Acknowledgments

The presented results were supported by the Deutsche Ministerium für projektträger Jülich under contract number 0329857B. Junfeng Han acknowledges financial support by the China scholarship council.

References

[1] K.L. Chopra, P.D. Paulson, V. Dutta, Progress in Photovoltaics: Research and Applications 12 (2004) 69–92.
[2] X. Mathew, J. Pantoja Enriquez, A. Romeo, A.N. Tiwari, Solar Energy 77 (2004) 831.
[3] A. Luque, S. Hegedus, Handbook of Photovoltaic Science and Engineering, John Wiley & Sons Ltd., England, 2003 (Chapter14).
[4] J. Touskova, D. Kindl, L. Dobiasova, J. Tousek, Solar Energy Materials and Solar Cells 53 (1998) 177–188.
[5] W. Jaegermann, A. Klein, J. Fritsche, D. Kraft, B. Späth, Materials Research Society Symposium Proceedings 865 (2005), F6.1.
[6] J. Fritsche, A. Klein, W. Jaegermann, Advanced Engineering Materials 7 (2005) 914–920.
[7] N. Romeo, A. Bosio, V. Canevari, A. Podesta, Solar Energy 77 (2004) 795–801.
[8] A. Romeoa, D.L. Bätznera, H. Zogga, C. Vignalib, A.N. Tiwari, Solar Energy Materials and Solar Cells 67 (2001) 311–321.
[9] J. Lee, Applied Surface Science 252 (2005) 1398–1403.

[10] X. Wu, J.C. keane, R.G. Dhere, C. DeHart, D.S. Albin, A. Duda, T.A. Gessert, S. Asher, D.H. Levi, P. Sheldon, Proceedings of the 17th European Photovoltaic Solar Energy Conference, Munich, Germany, October 22–26, 2001, p. 995.
[11] N. Romeo, A. Bosio, R. Tedeschi, V. Canevari, Materials Chemistry and Physics 66 (2000) 201–206.
[12] H.R. Moutinho, D. Albin, Y. Yan, R.G. Dhere, X. Li, C. Perkins, C.S. Jiang, B. To, M.M. Al-Jassim, Thin Solid Films 436 (2003) 175–180.
[13] M. Hädrich, N. Lorenza, H. Metznera, U. Reislöhnera, S. Macka, M. Gosslaa, W. Witthuhn, Thin Solid Films 515 (2007) 5804–5807.
[14] N. Romeoa, A. Bosio, V. Canevarib, M. Terheggenc, L. Vaillant Roca, Thin Solid Films 431–432 (2003) 364–368.
[15] J. Luschitz, K. Lakus-Wollny, A. Klein, W. Jaegermann, Thin Solid Films 515 (2007) 5814–5818.
[16] A. Morales-Acevedo, Solar Energy Materials and Solar Cells 90 (2006) 2213–2220.
[17] K. Durose, P.R. Edwards, D.P. Halliday, Journal of Crystal Growth 197 (3) (1999) 733–742, 15.
[18] M. Estela Calixto, M. Tufiño-Velázquez, G. Contreras-Puente, O. Vigil-Galán, M. Jiménez-Escamilla, R. Mendoza-Perez, J. Sastré-Hernández, A. Morales-Acevedo, Thin Solid Films 516 (2008) 7004–7007.
[19] J. Fritsche, A. Thissen, A. Klein, W. Jaegermann, Thin Solid Films 387 (2001) 158–160.
[20] P.K. Nair, O. Gomez Daza, A. Arias-Carbajal Readigos, J. Campos, M.T.S. Nair, Semiconductor Science and Technology 16 (2001) 651–656.
[21] X. Wu, Y. Yan, R.G. Dhere, Y. Zhang, J. Zhou, C. Perkins, B. To, Physica Status Solidi (c) 1 (2004) 1062–1066.